

Ventilated Metamaterial Absorber with High-efficiency Acoustic Absorption at Low Frequency

Xiaoxiao Wu^{1,a)}, Ka Yan Au-Yeung^{1,a)}, Xin Li², Robert Christopher Roberts³, Jingxuan Tian³,
Chuandeng Hu¹, Yingzhou Huang², Shuxia Wang², Zhiyu Yang¹, Weijia Wen^{1,b)}

¹*Department of Physics, The Hong Kong University of Science and Technology, Clear Water Bay, Kowloon, Hong Kong, China*

²*Department of Applied Physics, Chongqing University, Chongqing 401331, China*

³*Department of Mechanical Engineering, Faculty of Engineering, The University of Hong Kong, Hong Kong, China*

^{a)} Xiaoxiao Wu and Ka Yan Au-Yeung contributed equally to this work.

^{b)} To whom correspondence should be addressed. Electronic mail: phwen@ust.hk

ABSTRACT

We demonstrate a ventilated metamaterial absorber operating at low frequency. By employing only two layers of the absorption units, high-efficiency absorption is achieved in simulations ($> 90\%$) and experiments ($> 80\%$) at maximum absorption. This high-efficiency absorption is originated from the weak coupling of the two identical split tube resonators constituting the absorber, which leads to the hybridization of the degenerate eigenmodes and breaks the absorption upper limit of 50% for conventional transmissive symmetric acoustic absorbers. The absorber can also be extended to an array and work in free space. The absorber should have potential applications in acoustic engineering.

Absorbing low-frequency sounds is a long-standing challenge in acoustic researches. Conventional porous materials could not achieve high-efficiency absorption without a thickness comparable to the wavelength.^{1,2} To increase the absorption performance, we need to increase the density of states of acoustic waves at low frequency. Therefore, artificial structures, collectively called “metamaterials”, becomes popular in dealing with low-frequency sounds since they can support deep-subwavelength resonance modes and offer large density of states at low frequencies. Under this concept, many high-efficiency and subwavelength acoustic metamaterial absorbers have been proposed and realized over the last few years.³⁻⁹ Remarkably, an optimal acoustic metamaterial absorber has also been demonstrated.¹⁰ However, these high-efficiency absorbers all require reflectors, such as aluminum plates or rigid walls, which will unavoidably forbid fluid flows, such as air or water, to pass through these absorbers. If the reflectors of these absorbers are removed, their maximum absorption are usually limited to only 50%.^{11,12} In order to break this limit while maintaining no reflectors, several coherent perfect absorbers (CPAs), a concept originally adopted in optics as the time-reversal counterpart of lasers^{13,14}, have been proposed in acoustics.^{15,16} They can favorably achieve dynamic modulation of the acoustic absorption without changing any geometric structures. However, the corresponding dynamic generation and control of an extra incident acoustic beam is not easy and can be expensive in real applications, thus a passive high-efficiency ventilated absorber is still a more practical option. Recently, several ventilated absorbers have been proposed to meet this demand¹⁷⁻²¹, but most of them only achieve asymmetric one-sided high-efficiency absorption and are all proposed solely in the context of waveguides and could not be directly extended to an array of

absorbers which can work in free space. Therefore, it is desirable to develop a ventilated acoustic absorber which can achieve symmetric one-sided high-efficiency absorption in both waveguides and free space.

In this Letter, we demonstrate a ventilated metamaterial absorber (VMA) which can achieve symmetric one-sided high-efficiency absorption in simulations ($> 90\%$) and experiments ($> 80\%$). As the name suggests, the VMA permits the flow of fluids and also the transmission of acoustic waves at other frequencies. The VMA can work in a waveguide and can also be extended to an array which can work in free space.

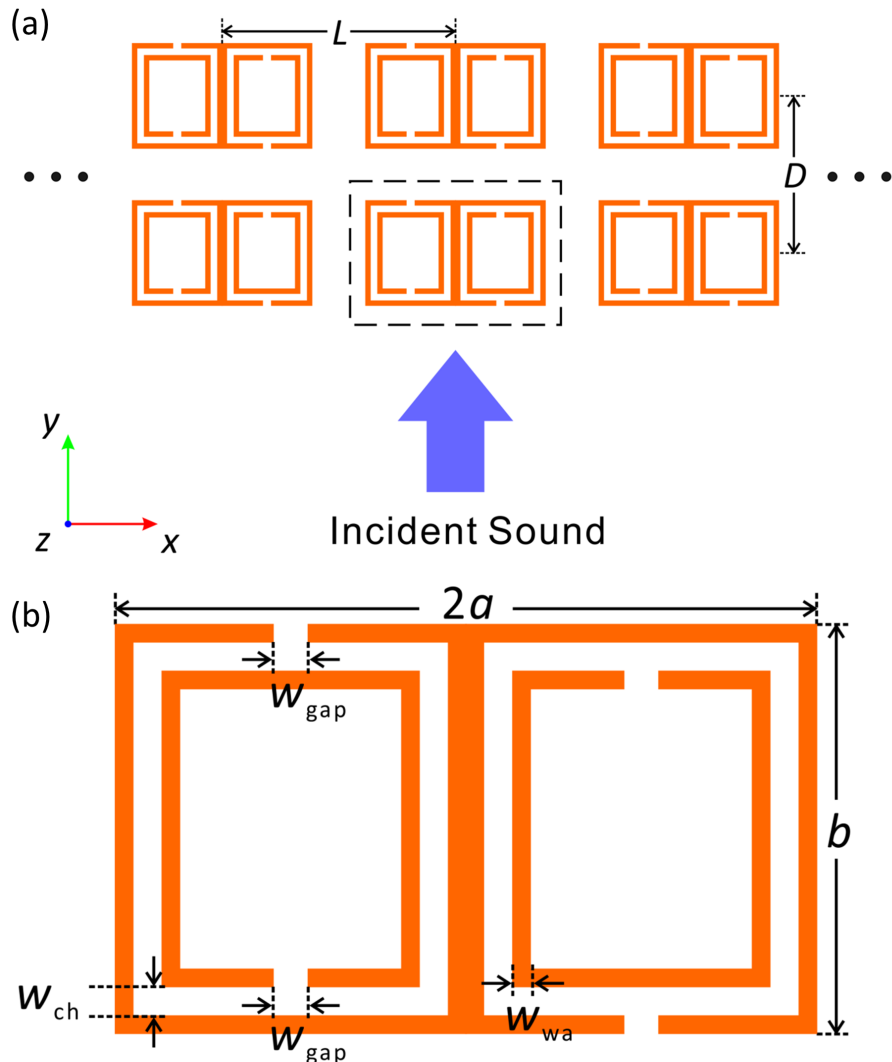


FIG. 1. Geometry of the designed ventilated metamaterial absorber (VMA). (a) Schematic

cross section illustrating the VMA composed of several layers of the absorption units which are invariant along the z direction. The dashed rectangle denote an absorption unit of the VMA. (b) Details of an absorption unit of the VMA, which is composed of two identical but oppositely oriented split tube resonators. A chosen set of the geometric parameters for demonstration purpose is listed in Table I.

As schematically depicted in Fig. 1(a), the designed VMA is composed of several layers of the absorption units arranged in a one-dimensional array along the x direction. In the array, an absorption unit is composed of two identical but oppositely oriented split tube resonators, which are invariant along the z direction, and the details of such a unit are shown in Fig. 1(b). For demonstration purpose, we choose a set of the geometric parameters for the VMA and they are listed in Table I.

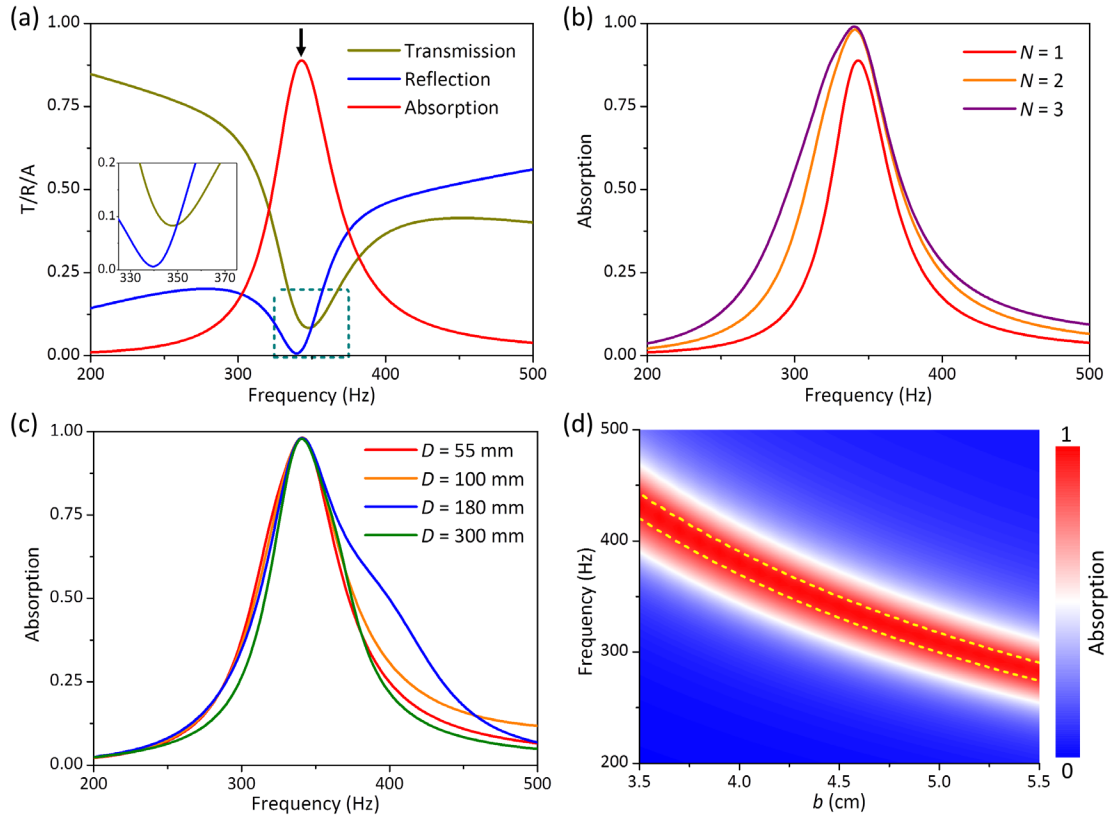


FIG. 2. Simulated acoustic performance of the VMA. (a) Simulated transmission(T)/reflection(R)/absorption(A) of the VMA composed of a single layer. The black arrow denotes the maximum absorption 88.7 % at 342 Hz (b) Simulated absorption of the VMA composed of N ($N = 1, 2, 3$) layers. $D = 55$ mm. (c) Simulated absorption of the VMA composed of two layers with varying distance D . (d) Simulated absorption of the VMA composed of two layers with varying thickness b . The dashed yellow lines denote the contour of 90% absorption.

We then examine the acoustic absorption performance of the VMA using COMSOL Multiphysics, a commercial Finite Element Method software package. As a starting point, we first consider a ventilated absorber comprising only one layer of the absorption units and assume that the absorber is immersed in air in simulations. Thermoacoustics, Frequency Domain (ta) module is used to simulate the friction inside the narrow channels of split tube resonators and other regions are simulated using Pressure Acoustics, Frequency Domain (acpr) module. In simulations, periodic boundary conditions are applied in the x direction and perfectly matched layers (PMLs) are applied in the y direction to truncate the simulation domain. The material properties of air are density $\rho = 1.2$ kg/m³, speed of sound $c = 343$ m/s, dynamic viscosity $\mu = 18.5$ μ Pa·s, thermal conductivity $k = 24$ mW·m⁻¹·K⁻¹, and heat capacity at constant pressure $C_p = 1000$ J·kg⁻¹·K⁻¹. No tunable parameters are involved in our simulations. The complex transmission coefficient t and reflection coefficient r are retrieved and the absorption coefficient A then is calculated as $A = 1 - T - R$ in which $T = |t|^2$ and $R = |r|^2$ because of the conservation of energy. Since the structure possesses spatial inversion

symmetry, the responses to the wave propagating along $+y$ or $-y$ directions are identical and hence we do not differentiate them (see also supplementary material). The simulation results are shown in Fig. 2(a), and it could be observed that a notable absorption ($\sim 88\%$) is achieved with only one layer of the absorption units at the frequency 342 Hz indicated by the black arrow. Similar to previous works^{5,8}, the energy dissipation is due to the large friction of the acoustic wave at the narrow necks of the split tube resonators caused by the pressure differences between the interior cavities and outside environment. Obviously, by adjusting the geometric parameters, the maximum absorption frequency could be precisely tuned to other desirable working frequencies.

TABLE I. Geometric parameters of the designed VMA, chosen for demonstration purpose.

All parameters are in unit of mm.

L	a	b	w_{ch}	w_{gap}	w_{wa}
90	35	45	1.6	1.6	2

Further, we can observe that near the maximum absorption frequency the reflection is very small ($< 0.7\%$) but the transmission is not negligible ($\sim 8.3\%$), as displayed in the inset of Fig. 2(a), which leads to a fair maximum absorption. This power distribution of the transmission and reflection reminds us that we can further increase the absorption by directly adding more layers of the absorption units. To verify this deduction, we simulated the absorption of the VMA composed of more layers. The simulated results are summarized in Fig. 2(b) and it can be seen that a near-unity ($> 98\%$) absorption has been achieved when there are only two layers of such absorption units. Further, when placing three layers, an

absorption $> 99\%$ is achieved. Because the absorption is due to the localized mode of the split tube resonators, the distance between each layer should not substantially affect the absorption performance. For proof, the simulated absorptions of the two layers of the absorption units are shown in Fig. 2(c) and there are no notable differences between these results corresponding to considerably different distances D , especially near the maximum absorption frequency. It should be emphasized that this high-efficiency absorption is not accidentally achieved due to our specifically chosen geometric parameters, but can be achieved for a wide range of the geometric parameters. For example, we consider a VMA composed of two layers of the absorption units and adjust the thickness of absorption unit b , while other geometric parameters are identical with those in Table I. The simulated absorption is plotted as a contour map against the thickness b and the frequency in Fig. 2(d), and 90% absorption is denoted by the yellow dashed lines. As can be seen from the contour map, the high-efficiency absorption is robust when we adjust the thickness of the absorption units. The maximum absorption frequency is shifted but the maximum absorption is larger than 90%, which suggests that we can customize the absorption units for specific frequencies. We also calculate the flow resistivity of the VMA in the waveguide and free space, and the results show that the effective flow resistivity ($< 10 \text{ Pa}\cdot\text{s}\cdot\text{m}^{-2}$) is much smaller compared with conventional porous materials ($2000\text{-}40000 \text{ Pa}\cdot\text{s}\cdot\text{m}^{-2}$)²² and hence the VMA will not observably impede the air flow (see supplementary material).

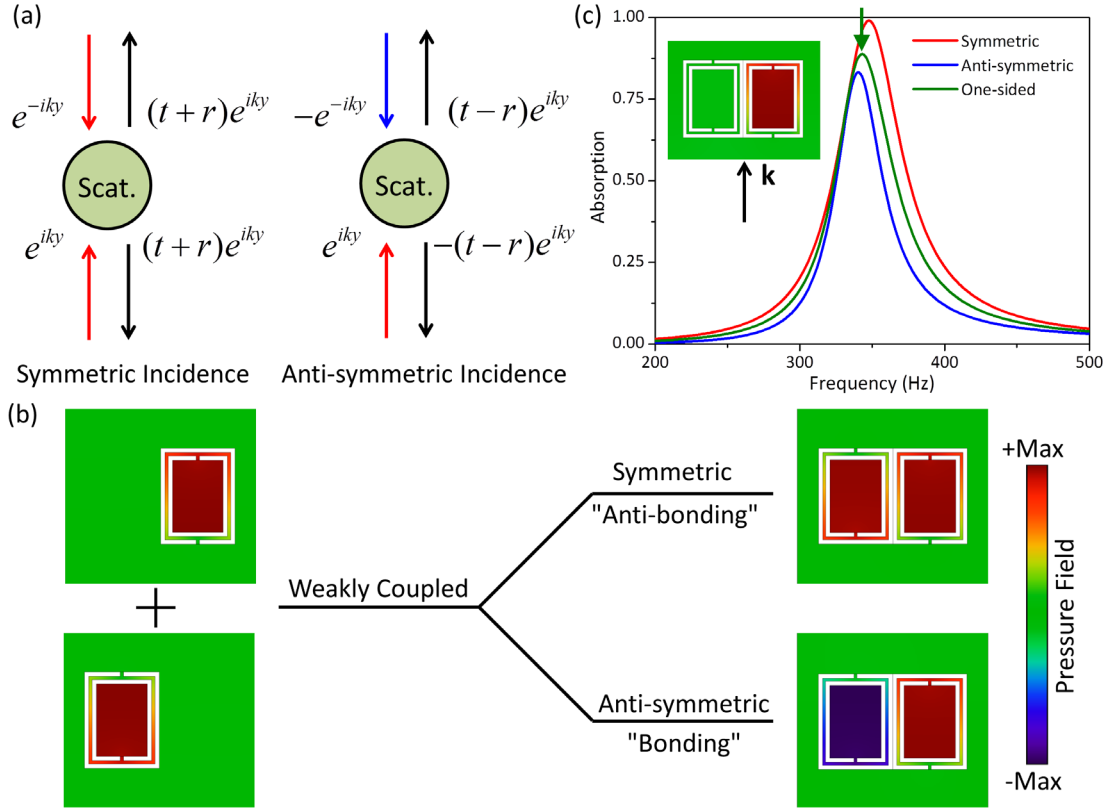


FIG. 3. Origin of symmetric high-efficiency absorption of the VMA. (a) Schematic sketches illustrating the situation of (left) symmetric incidence and (right) anti-symmetric incidence. “Scat.” stands for “Scatter”. (b) Diagram of the frequency split of the two weakly coupled split tube resonators. The degenerate eigenmodes of the two split tube resonators are split into a symmetric mode with a higher frequency (“Anti-bonding”) 346 Hz and an anti-symmetric mode with a lower frequency (“Bonding”) 339 Hz. (c) Simulated symmetric absorption A_s , anti-symmetric absorption A_a , and one-sided absorption A of the VMA. The inset shows the snapshot of the pressure field of the VMA at 342 Hz as indicated by the green arrow under one-sided incidence (incident from $-y$ direction) as denoted by the black arrow.

In order to understand why this subwavelength absorber with inversion symmetry could achieve absorption notably larger than 50%, we briefly review why conventional

subwavelength absorber with inversion or mirror symmetry could not achieve absorption larger than 50%. For convenience, we consider a reciprocal scattering process in an one-dimensional system with two ports and assume that the scatter is symmetric with respect to the two ports. In such configuration, the scattering process could be described using a scattering matrix $\mathbf{S}(f)$ which relates the phasors of the incoming waves $[a, b]^T$ to the phasors of the outgoing waves $[c, d]^T$

$$\begin{bmatrix} c \\ d \end{bmatrix} = \mathbf{S}(f) \begin{bmatrix} a \\ b \end{bmatrix} = \begin{bmatrix} t & r \\ r & t \end{bmatrix} \begin{bmatrix} a \\ b \end{bmatrix}, \quad (1)$$

in which t and r are the complex transmission and reflection coefficients of the scatter, as aforementioned.¹⁹ We can simply verify that the eigenvalues of $\mathbf{S}(f)$ is ± 1 , which corresponds to a symmetric incidence $[1, 1]^T$ or an anti-symmetric incidence $[1, -1]^T$, respectively. The scattering processes of symmetric incidence and anti-symmetric incidence are sketched in Fig. 3(a). We can then decompose the one-sided incidence $[1, 0]^T$ into a superposition of the symmetric incidence and anti-symmetric incidence.¹⁵ This decomposition inspires us to rewrite the expression of the absorption A as¹⁹

$$A = 1 - |r|^2 - |t|^2 = \frac{1 - |r+t|^2 + 1 - |r-t|^2}{2} = \frac{1}{2}(A_s + A_a), \quad (2)$$

in which the second equal sign is due to the identity $|r+t|^2 + |r-t|^2 = 2(|r|^2 + |t|^2)$. Further, as sketched in Fig. 3(a), $A_s = 1 - |r+t|^2$ is the absorption under symmetric incidence, while $A_a = 1 - |r-t|^2$ is the absorption under anti-symmetric incidence. For convenience, we simply call A_s and A_a as symmetric and anti-symmetric absorption, respectively. Because of the conservation of energy, for a passive scatter, we have the following constraints

$$0 \leq A_a \leq 1, \quad (3)$$

and

$$0 \leq A_s \leq 1. \quad (4)$$

When the scatter has an inversion center or a mirror axis perpendicular to the wave propagating direction, its eigenmodes will be symmetric or anti-symmetric under the symmetry operation. It can be proven that for subwavelength scatters, a symmetric eigenmode will be transparent for anti-symmetric incidence ($A_a = 0$) and an anti-symmetric eigenmode will be transparent for symmetric incidence ($A_s = 0$). If the subwavelength scatter only have a symmetric or anti-symmetric eigenmode in the considered frequency range, it will only have symmetric absorption A_s or anti-symmetric absorption A_a . As a direct result of Eqs. (3) and (4), its one-sided absorption $A = A_s/2$ or $A = A_a/2$ then cannot exceed 50% in this frequency range. Similar conclusions have been proven and demonstrated for several specific acoustic absorbing structure in previous works.^{12,19}

However, because here we have two weakly coupled identical split tube resonators, their degenerate eigenmodes will interact with each other and be split into a symmetric mode with a higher eigenfrequency (“Anti-bonding”) at 339 Hz and an anti-symmetric mode with a lower eigenfrequency (“Bonding”) at 346 Hz, as shown in Fig. 3(b). We further extract the symmetric absorption A_s and anti-symmetric absorption A_a of the VMA from simulations, and plot them as well as the one-sided absorption A in Fig. 3(c). It can be observed that both symmetric and anti-symmetric eigenmodes are well excited under two-sided incidence and these two absorption peaks are very close and overlap with each other. The coexistence of large symmetric and anti-symmetric absorptions then ensures that our absorber can achieve a high-efficiency absorption at the frequency (342 Hz) between two eigenmodes. The inset shows the snapshot of the pressure field of the VMA when the wave is incident from $-y$

direction and it can be observed that the pressure in the left split tube resonator is very small, indicating that the excited field inside the VMA under one-side incidence is indeed a linear superposition of the symmetric and anti-symmetric mode.

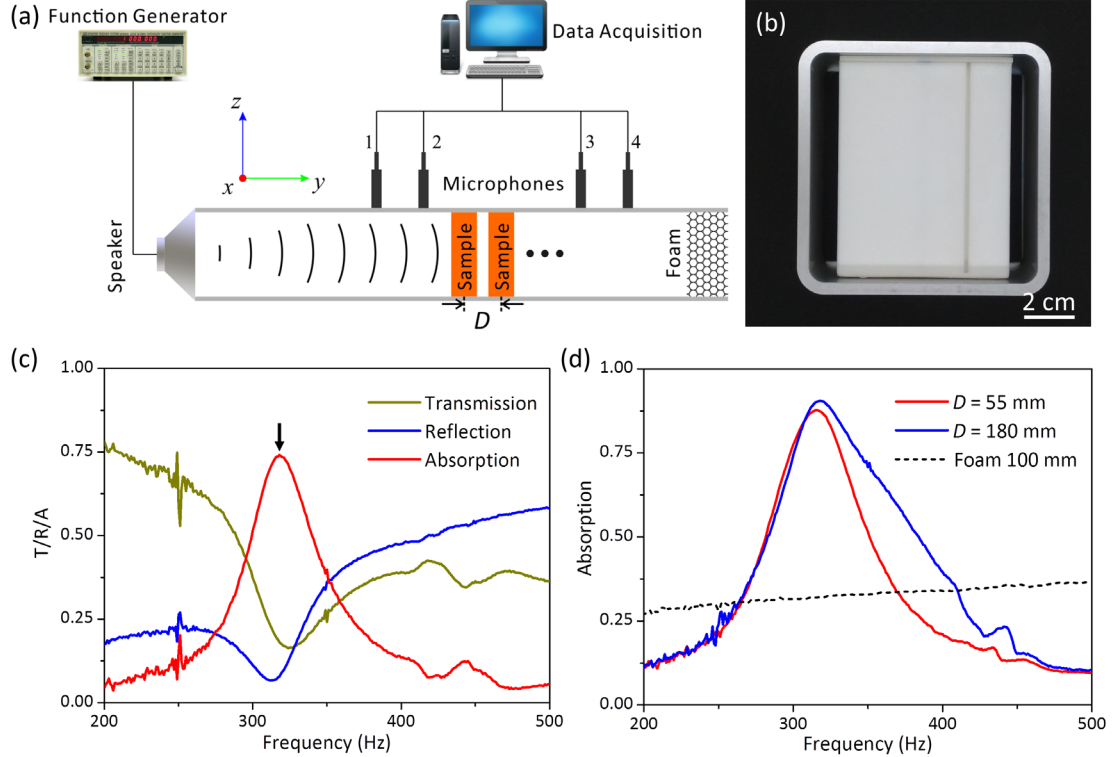


FIG. 4. Experimental characterization of the VMA. (a) Experiment set-up. (b) Photograph of a fabricated sample mounted in a section of the impedance tube. (c) Measured transmission(T)/reflection(R)/absorption(A) of a single absorption unit. The black arrow denotes the maximum absorption 74.1% at 318 Hz. (d) Measured absorption A of the VMA comprising two absorption units with varied distance D and also the reference sample, which is a piece of foam with thickness 100 mm, width 70 mm, and height 90 mm. The maximum absorption reaches 87.8% ($D = 55$ mm) and 90.5% ($D = 180$ mm), respectively.

After understanding its working mechanism, to experimentally confirm the VMA, we measure the acoustic performance of its absorption unit under normal incidence in a square

impedance tube.⁸ The side length of the cross section of the square impedance tube is 90 mm, corresponding to a plane wave cutoff frequency ~ 1900 Hz. We use the standard four-microphone method to measure the complex transmission coefficient t and reflection coefficient r , and the schematic diagram of the experiment setup is shown in Fig. 4(a). More detailedly, a function generator is used to excite the speaker mounted at one end of the impedance tube and a thick piece of foam is placed at the other end to suppress unwanted reflections. The four microphones inserted in the impedance tube are connected to a computer through a data acquisition card. Samples which are absorption units of the VMA are mounted in the middle of the impedance tube between microphones 1, 2 and microphones 3, 4, and these samples in experiments are made from polylactide (PLA) plastic by 3D printing techniques. The photograph of such a sample mounted on a section of the impedance tube is shown in Fig. 4(b). Time-domain data are collected by the four microphones and then fast Fourier transformed on the connected computer to calculate the complex transmission coefficient t and reflection coefficient r in frequency domain. The experimental absorption coefficient A then is calculated as $A = 1 - T - R$ with $T = |t|^2$ and $R = |r|^2$, the same as the simulations. In experiments, we first measure the acoustic performance of a single unit and the result are shown in Fig. 4(c). It can be observed that the measured results agree well with the simulated results in Fig. 2(a), though the maximum absorption in experiments is slightly lower than simulated ones. This discrepancy could be attributed to the fact that the PLA plastic we use to print the samples are not completely rigid. Therefore, the pressure difference between the Helmholtz resonators and the ambient environment is overestimated in simulations, which in turn leads to the slight overestimation of the absorption performance in

simulations. The fabrication tolerance (± 0.2 mm) could also contribute to the discrepancy since it is not small compared with the width of the channel ($w_{ch} = 1.6$ mm). Nevertheless, the measured results still suggest that the VMA can achieve absorption notably higher than 50% and the low reflection suggests that we can enhance the absorption by simply adding more layers. We then measure the performance of two units with the distances $D = 55, 180$ mm, respectively, and the results are plotted in Fig. 4(d). It can be seen that both results also agree well with the corresponding simulations results shown in Fig. 2(c), and confirm that adding more layers is feasible for improving the absorption of the VMA. For reference, we have also measured the absorption of a piece of foam with its thickness, width, and height being 100 mm, 70 mm, 90 mm, respectively, and the result is plotted as the black dashed line in Fig. 4(d). It can be observed that the absorption of the VMA is much more efficient in a broadband near the resonant modes compared with the foam as expected.

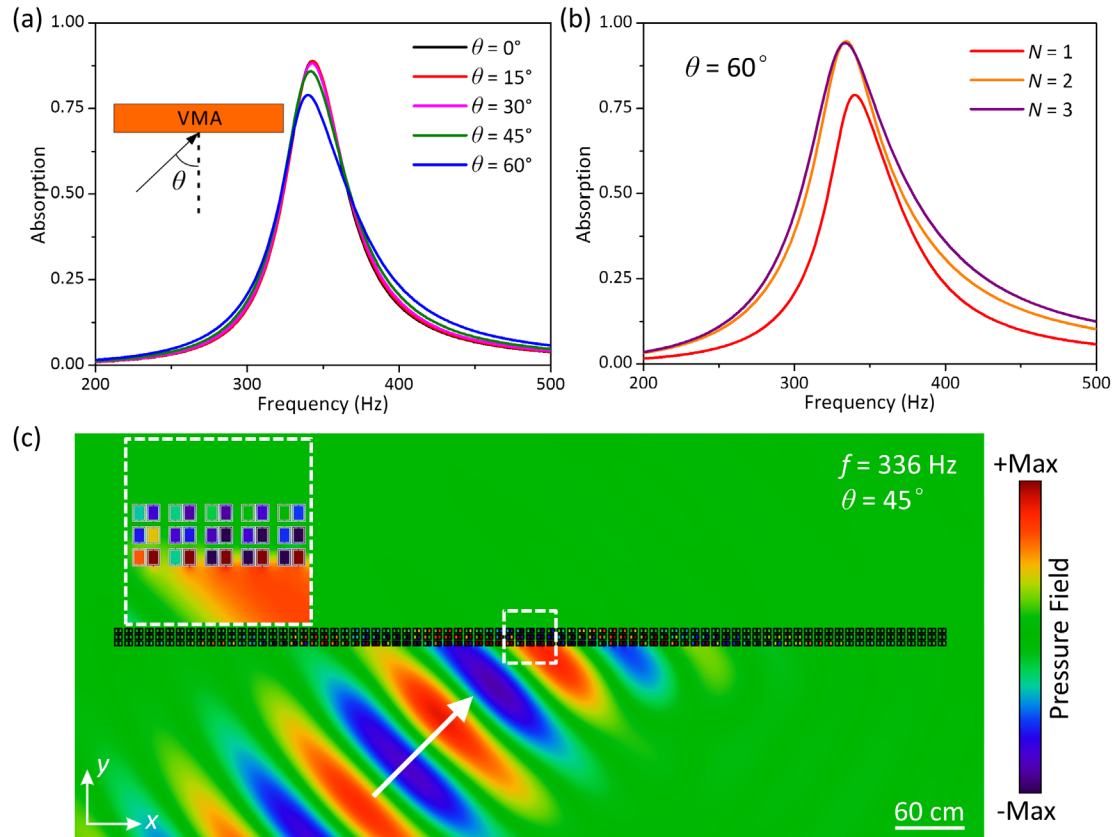


FIG. 5. Simulated performance of VMAs under oblique incidence in free space. (a) Simulated absorption of a single layer under oblique incidence. The inset defines the angle of incidence θ . (b) Simulated absorption of the VMA comprising N ($N = 1, 2, 3$) layers of the absorption units. The distance between each layer is $D = 55$ mm. (c) Simulated pressure field at 336 Hz when a two-dimensional Gaussian beam impinges on a VMA comprising three layers of absorption units in free space. The distance between each layer is $D = 55$ mm. The propagating direction of the beam is indicated by the white arrow and the angle of incidence is 45° . The inset shows the enlarged field distribution of the region enclosed by the white dashed rectangle.

As we have experimentally validated the VMA, we further estimate its performance under oblique incidence which is important for applications in free space. We plot the simulated absorptions of a single layer under various angles of incidence θ in Fig. 5(a), with θ defined in the inset. It can be observed that there is no significant degradation of absorption performance under oblique incidence with θ up to 60° . We also calculate the absorption of two layers of the absorption units under oblique incidence and the results shown in Fig. 5(b) also suggest that the VMAs can maintain a satisfying performance under oblique incidence in free space. Further, to directly visualize its performance in free space, we consider a two-dimensional Gaussian beam of acoustic waves impinging on a VMA composed of 3 layers with $D = 55$ mm. The waist radius of the beam is 1 m and the angle of incidence is 45° . A snapshot of the simulated pressure field at the frequency 336 Hz is shown in Fig. 5(c). It can be seen that no notable reflection or transmission is generated after the beam encounters

the VMA, which indicate a high-efficiency absorption of the incident beam at this frequency.

At lower frequencies, the VMA is mainly transmissive, while at higher frequencies, the VMA is mainly reflective, as indicated in Fig. 2(a) (see also supplementary material).

Finally, we point out that though we only demonstrate VMAs for audible sound in air, the design can be correspondingly modified for applications in other frequency regimes and fluids, such as sonar sound (kHz) in water (see supplementary material), only requiring that it is made of materials rigid enough compared with the ambient environment. For example, when applied in water, the VMA should be made of brass or stainless steel, rather than plastics.

To summarize, we have demonstrated a ventilated acoustic absorber without any elastic membranes which can achieve high-efficiency absorption while maintaining a subwavelength thickness. The working frequency and absorption performance of the absorber is largely independent of its material properties and can be tuned by adjusting its geometry parameters. The absorber should be useful for applications which require both noise reduction and ventilation. The absorber can be scaled for applications in other working frequency regimes and fluids.

SUPPLEMENTARY MATERIAL

See supplementary material for confirmation of symmetric acoustic performance of the VMA, the flow resistivity of the VMA of different sizes, transparency of eigenmodes under symmetric or anti-symmetric incidence, pressure fields of the VMA under oblique incidence in free space at other frequencies, and realization of the VMA in other working frequency

regimes and fluids.

ACKNOWLEDGEMENT

The project is supported by an Areas of Excellence Scheme grant (AOE/P-02/12) from research grant council (RGC) of Hong Kong and the Special Fund for Agro-scientific Research in the Public Interest from Ministry of Agriculture of the Peoples' Republic of China (no. 201303045).

REFERENCES

- ¹ Min Yang and Ping Sheng, *Annual Review of Materials Research* **47**, 83 (2017).
- ² Guancong Ma and Ping Sheng, *Science advances* **2** (2), e1501595 (2016).
- ³ Guancong Ma, Min Yang, Songwen Xiao, Zhiyu Yang, and Ping Sheng, *Nature Materials* **13** (9), 873 (2014).
- ⁴ Xiaobing Cai, Qiuquan Guo, Gengkai Hu, and Jun Yang, *Applied Physics Letters* **105** (12), 121901 (2014).
- ⁵ Junfei Li, Wenqi Wang, Yangbo Xie, Bogdan-Ioan Popa, and Steven A Cummer, *Applied Physics Letters* **109** (9), 091908 (2016).
- ⁶ Chi Zhang and Xinhua Hu, *Physical Review Applied* **6** (6), 064025 (2016).
- ⁷ Yong Li and Badreddine M Assouar, *Applied Physics Letters* **108** (6), 063502 (2016).
- ⁸ Xiaoxiao Wu, Caixing Fu, Xin Li, Yan Meng, Yibo Gao, Jingxuan Tian, Li Wang, Yingzhou Huang, Zhiyu Yang, and Weijia Wen, *Applied Physics Letters* **109** (4), 043501 (2016).

⁹ Changru Chen, Zhibo Du, Gengkai Hu, and Jun Yang, *Applied Physics Letters* **110** (22), 221903 (2017).

¹⁰ Min Yang, Shuyu Chen, Caixing Fu, and Ping Sheng, *Materials Horizons* (2017).

¹¹ Min Yang, Yong Li, Chong Meng, Caixing Fu, Jun Mei, Zhiyu Yang, and Ping Sheng, *Comptes Rendus Mécanique* **343** (12), 635 (2015).

¹² Min Yang, Guancong Ma, Zhiyu Yang, and Ping Sheng, *EPJ Applied Metamaterials* **2**, 10 (2015).

¹³ YD Chong, Li Ge, Hui Cao, and A Douglas Stone, *Physical review letters* **105** (5), 053901 (2010).

¹⁴ Jianfa Zhang, Kevin F MacDonald, and Nikolay I Zheludev, *Light: Science & Applications* **1** (7), e18 (2012).

¹⁵ Pengjiang Wei, Charles Croënne, Sai Tak Chu, and Jensen Li, *Applied Physics Letters* **104** (12), 121902 (2014).

¹⁶ JZ Song, P Bai, ZH Hang, and Yun Lai, *New Journal of Physics* **16** (3), 033026 (2014).

¹⁷ Min Yang, Chong Meng, Caixing Fu, Yong Li, Zhiyu Yang, and Ping Sheng, *Applied Physics Letters* **107** (10), 104104 (2015).

¹⁸ Caixing Fu, Xiaonan Zhang, Min Yang, Songwen Xiao, and Z Yang, *Applied Physics Letters* **110** (2), 021901 (2017).

¹⁹ A Merkel, G Theocharis, O Richoux, V Romero-García, and V Pagneux, *Applied Physics Letters* **107** (24), 244102 (2015).

²⁰ Noé Jiménez, Vicent Romero-García, Vincent Pagneux, and Jean-Philippe Groby, *Scientific Reports* **7** (1), 13595 (2017).

²¹ Houyou Long, Ying Cheng, and Xiaojun Liu, *Applied Physics Letters* **111** (14), 143502 (2017).

²² Trevor J Cox and Peter D'antonio, *Acoustic absorbers and diffusers: theory, design and application*. (CRC Press, 2009).